LA-7533-MS
Informal Report

Evaluation of n + ^{242}Pu Reactions from 10 keV to 20 MeV

LOS ALAMOS SCIENTIFIC LABORATORY
Post Office Box 1663 Los Alamos, New Mexico 87545

UNITED STATES
DEPARTMENT OF ENERGY
CONTRACT W-7405-ENG. 36

LA-7533-MS
Informal Report

UC-34c
Issued: October 1978

Evaluation of n + ^{242}Pu Reactions from 10 keV to 20 MeV

D. G. Madland
P. G. Young

EVALUATION OF n + ^{242}Pu REACTIONS FROM 10 keV to 20 MeV

by

D. G. Madland and P. G. Young

ABSTRACT

An evaluation of the n + ^{242}Pu cross sections is presented for the neutron energy range of 10 keV to 20 MeV. The total fission and radiative capture cross sections are based upon experimental measurements on ^{242}Pu. The remaining cross sections, together with the elastic and inelastic angular distributions to low-lying states, have been calculated using various reaction models. An expression is presented for the energy dependence of the average number of neutrons produced per fission. The results have been placed in ENDF/B-V format and combined with a recent evaluation of data below 10 keV by the Hanford Engineering Development Laboratory, so that a complete data set covering the energy range of 10^{-5} eV to 20 MeV is available.

I. INTRODUCTION

A new evaluation of the n + ^{242}Pu cross sections has been completed for the neutron energy range of 10 keV to 20 MeV. The evaluation relies to a large extent upon nuclear model calculations as experimental data exist only for the fission and radiative capture cross sections within this energy range. The capture cross-section measurements, moreover, extend only to 90 keV. Model calculations were therefore used to derive the total, elastic, inelastic, (n,xn), and (n,γ) cross sections, as well as the elastic and inelastic angular distributions. The calculated first-, second-, and third-chance fission cross sections [(n,xnf) reactions] were also used in the evaluation.

An expression is presented for the energy dependence of the average number of neutrons per fission, $\bar{\nu}$, which is based upon existing phenomenological formulae

and $\bar{\nu}$ measurements for the neighboring n + ^{240}Pu system. Parameterizations are given for the inelastic, (n,xn), and fission neutron spectra that are consistent with the model calculations and the $\bar{\nu}$ representation.

The complete evaluation, including uncertainty estimates for the cross-section files, has been placed in ENDF/B-V format and combined with data below 10 keV from a recent evaluation by Mann and Schenter[1] at Hanford Engineering Development Laboratory (HEDL). The resulting data set, covering the energy range 10^{-5} eV to 20 MeV, has been provided to the National Nuclear Data Center at Brookhaven National Laboratory.

Details of the model calculations are presented in Sec. II together with a discussion of parameter sensitivities. The available experimental data are described in Sec. III and compared to the present recommended cross sections. In addition, the calculated cross sections for unmeasured reactions are presented for comparison with three other evaluations. Finally, a summary is contained in Sec. IV, together with conclusions and recommendations based upon our analysis.

II. MODEL CALCULATIONS

The only reaction for which it was possible to rely entirely upon measurements for the evaluation was the fission cross section. For all other reactions, nuclear model calculations were used to determine the recommended data. In this section a description is given of the optical model, direct coupled-channel, and compound-nucleus Hauser-Feshbach calculations used in the evaluation.

A. Optical Potential

All calculations described below use a preliminary version of a global actinide potential for neutrons that is under development at the Los Alamos Scientific Laboratory (LASL).[2] This potential is based upon an analysis of measured neutron total cross sections and elastic angular distributions between 1 keV and 19.9 MeV for ^{233,235,238}U. The parameterization of the Saxon-Woods form factors is listed in Table I.

The present potential does not include nuclear deformation effects, that is, it is a spherical optical potential. Ultimately, it will serve as the starting point in the derivation of a deformed optical potential that will account directly for the strong collective rotational effects observed in the actinide nuclei, and measured inelastic angular distributions will be included in that analysis. For the present evaluation, however, the effects of nuclear deformation are incorporated in an ad hoc manner, as described in Secs. II.B and III.F.

For purposes of comparison and because no elastic or total cross-section data exist for n + ^{242}Pu above 10 keV, calculations of the total, shape elastic, and reaction cross sections using the preliminary potential of Table I are compared to those of other neutron-nucleus global optical potentials in Figs. 1-3. The comparison potentials are the Wilmore-Hodgson potential,[3] the Becchetti-Greenlees potential,[4] and the Perey potential.[5] Of the four potentials, only the preliminary potential (Table I) is restricted to actinide data, whereas the others were derived for larger ranges of A. The figures give an example of the dispersion of values that can be obtained in calculating these cross sections in the absence of experimental data. The widest dispersions generally occur at lower energies and, in particular, the calculated reaction cross sections differ by as much as $\sim$60% at $\sim$100 keV. The latter appears to be partly due to the wide variation observed in the calculated compound elastic scattering (not plotted) in the energy range 10 keV to $\sim$2 MeV.

It is known that the potential of Table I reproduces the total and elastic (and therefore reaction) cross sections for ^{233,235,238}U in the energy range 10 keV to $\leqslant$ 2 MeV fairly well.[2] Therefore, insofar as ^{242}Pu behaves similarly, the Table I potential should also represent the n + ^{242}Pu cross sections reasonably well. Above 1-2 MeV, the nuclear deformation effects are strong,[6] and since each of the four global potentials is spherical, such effects must be added ad hoc in every case. In the present calculations, the use of the Table I potential is retained in this energy region to maintain continuity with the lower energy region.

B. Direct Reaction Coupled-Channel Calculations

The direct coupled-channel inelastic scattering was calculated with the code JUKARL, which is the LASL version of JUPITOR -- KARLSRUHE SEARCH VERSION.[7] Elastic and inelastic scattering to the first five members of the ground-state rotational band (see Table II) were calculated assuming a deformed axially symmetric rotator model for the ^{242}Pu target. The quadrupole (β_2) and hexadecapole (β_4) deformations used were extracted from E2 and E4 transition strengths obtained in Coulomb excitation measurements[8] of the ^{242}Pu 2^+ and 4^+ states using 17-MeV alpha particles (see Table II).

With these deformations, the optical potential of Table I was transformed to the total interaction potential for the coupled-channels calculation by use of the appropriate collective radius expression,

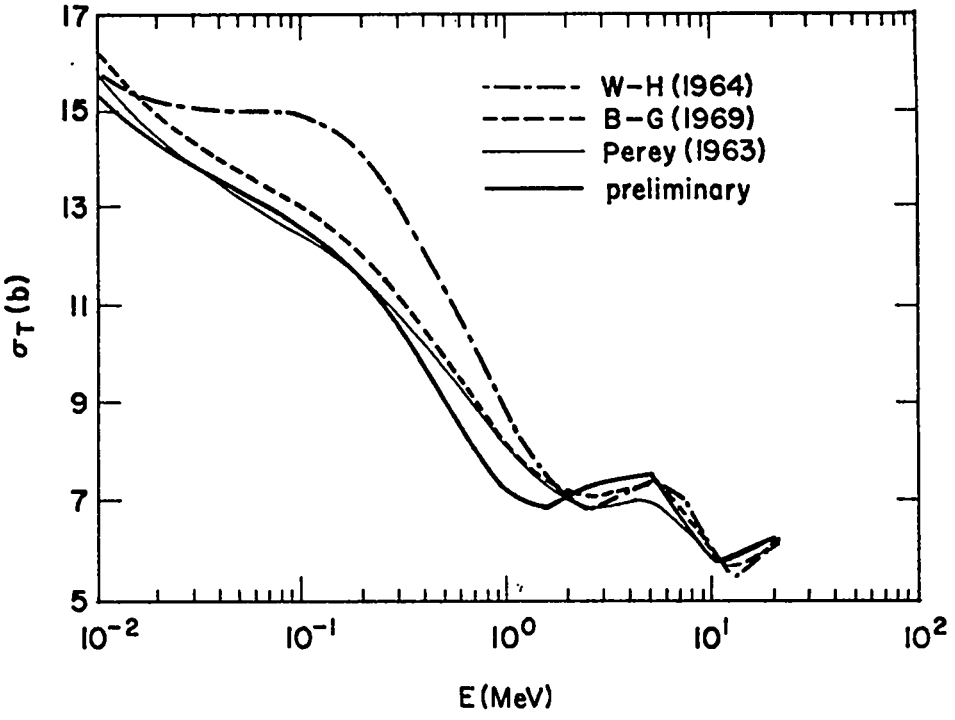

Fig. 1.
The n + ^{242}Pu total cross section calculated from the preliminary actinide potential,[2] the Wilmore-Hodgson potential,[3] the Becchetti-Greenlees potential,[4] and the Perey potential.[5]

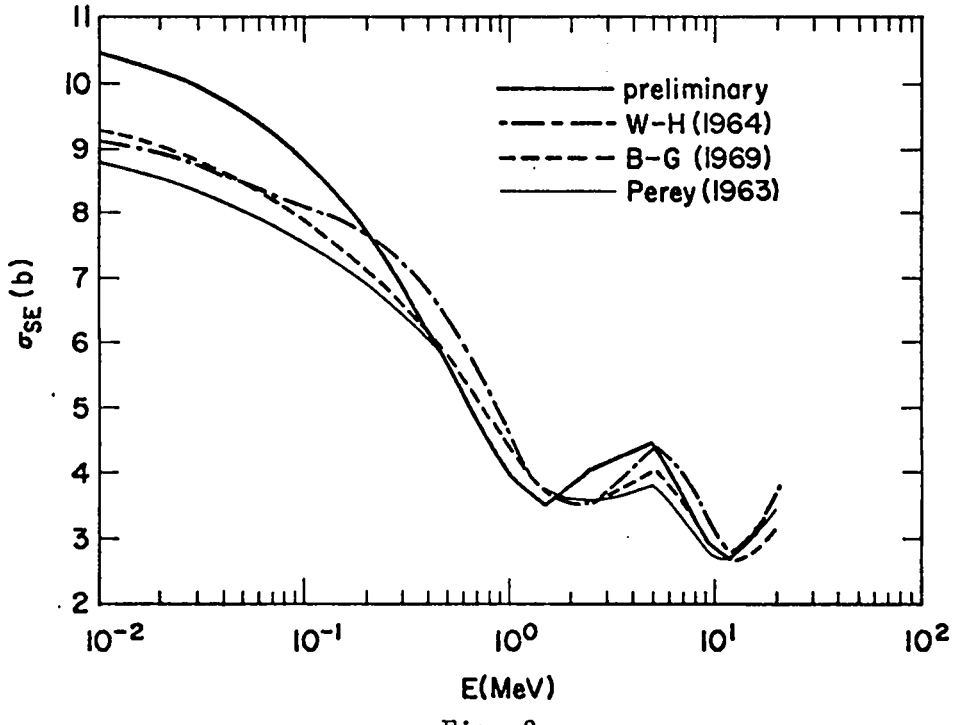

Fig. 2.
The n + ^{242}Pu shape elastic cross section calculated from four different optical potentials (see caption to Fig. 1).

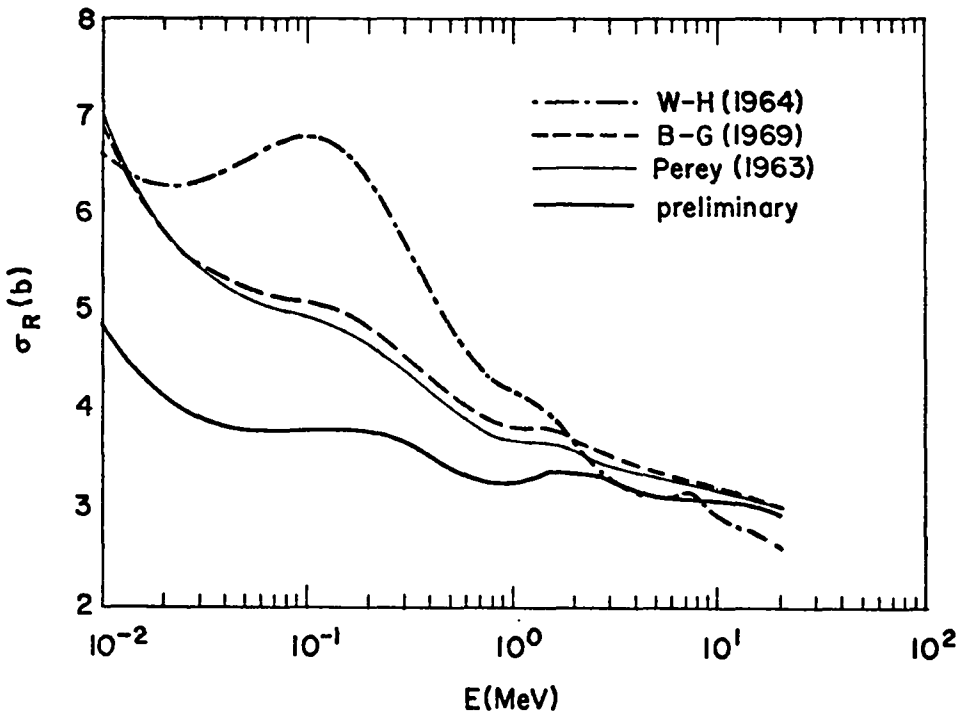

Fig. 3.
The n + ^{242}Pu reaction cross section calculated from four different optical potentials (see caption to Fig. 1).

$$R \rightarrow R\left[1 + \beta_2 Y_{20}(\theta) + \beta_4 Y_{40}(\theta)\right] \quad , \tag{1}$$

where R is the half-radius ($r_R A^{1/3}$ or $r_I A^{1/3}$) of either the real or imaginary part of the potential, β_L are the nuclear deformations, and θ refers to the body-fixed system.* The actual calculations utilized complex form factors at all energies and, at a given energy, used the same form factor for all channels. The adiabatic coupling approximation was used above 600 keV in order to minimize computing time.

The direct inelastic cross sections obtained for the first four excited states of the ground band are illustrated in Figs. 4-7 and compared to the compound-nucleus components (see Sec. II.C). Finally, the sum of the direct inelastic and total compound-nucleus inelastic cross section is shown in Fig. 8. The contribution of the direct to the total inelastic scattering is relatively small up to a neutron energy of ∿8 MeV, after which it becomes dominant.

*Ideally, the β_L's and the optical potential are determined simultaneously, assuming the existence of a complete data set. As no data exist, this procedure is not possible for the present calculation.

TABLE I

PRELIMINARY SPHERICAL GLOBAL OPTICAL POTENTIAL FOR THE ACTINIDES* (1 keV $\leq$ En $\leq$ 20 MeV)

$V_R = 53.016 - 0.344\ E_L - 24.5$

$r_R = 1.203 \qquad a_R = 0.300 + 1.492\ \eta$

$W_V = -0.566 + 0.210\ E_L$ (or zero, whichever is greater)

$W_D = 8.905 - 0.255\ E_L - 13.6\ \eta$

$r_I = 1.306$

$a_I = 0.250 + 0.733\ (E_L/100) + 1.420\ \eta$

$V_{SO} = 6.20$

$r_{SO} = 1.01 \qquad a_{SO} = 0.75$

$\eta = (N-Z)/A$

*Units are MeV and fermis.

TABLE II

PARAMETERS FOR DIRECT INELASTIC COUPLED-CHANNEL CALCULATIONS FOR ^{242}Pu

States Coupled:	J^π	K	Excitation (keV)
	0^+	0	0.00
	2^+	0	44.54
	4^+	0	147.20
	6^+	0	305.90
	8^+	0	517.60

Deformations: $\beta_2 = 0.260 \pm 0.010$

$\beta_4 = 0.036 \pm 0.037$

Reference 16

Optical Potential: Table I

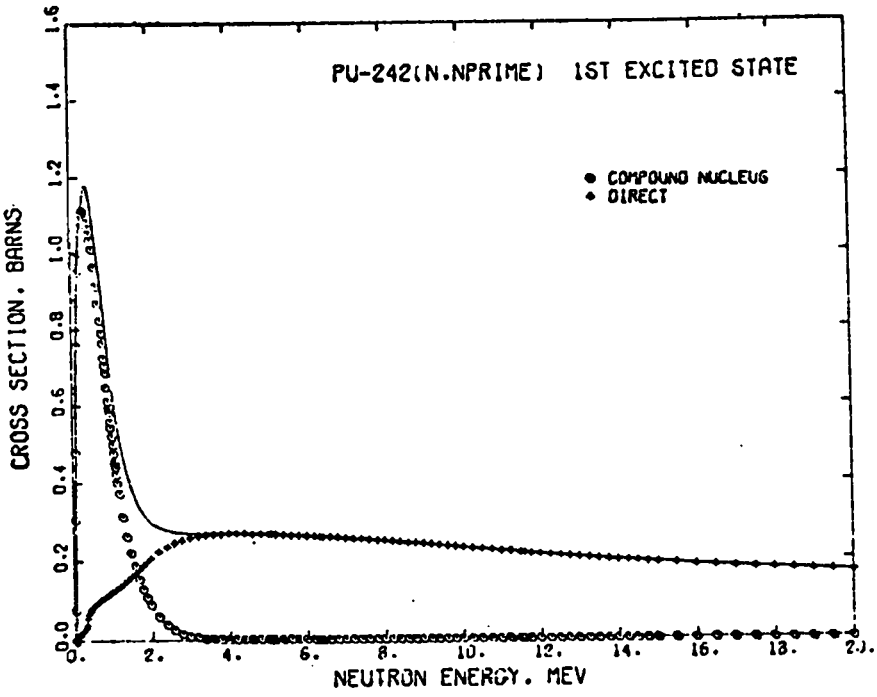

Fig. 4.
Calculated compound nucleus, direct, and total inelastic cross section to the first excited state of ^{242}Pu.

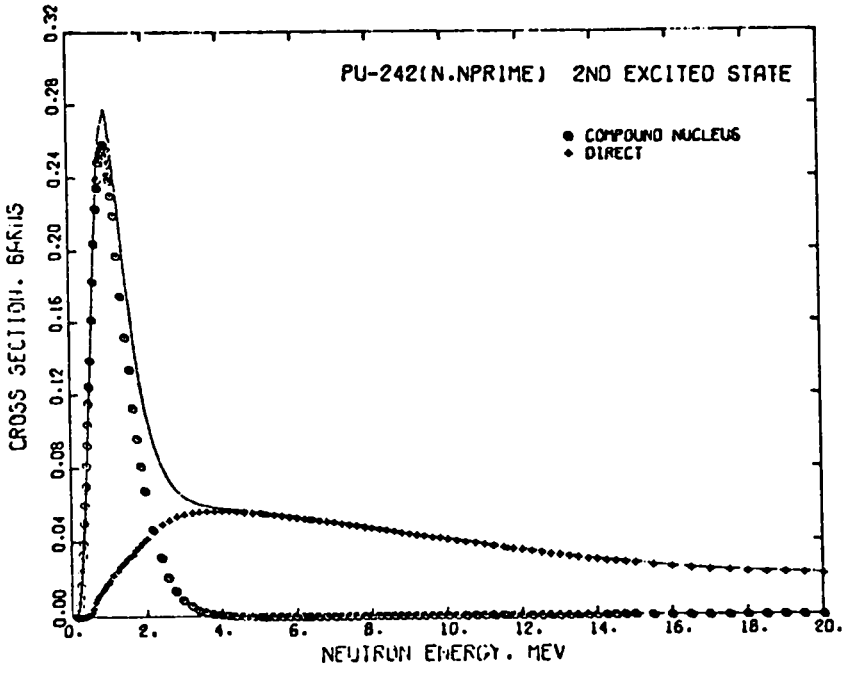

Fig. 5.
Calculated compound nucleus, direct, and total inelastic cross section to the second excited state of ^{242}Pu.

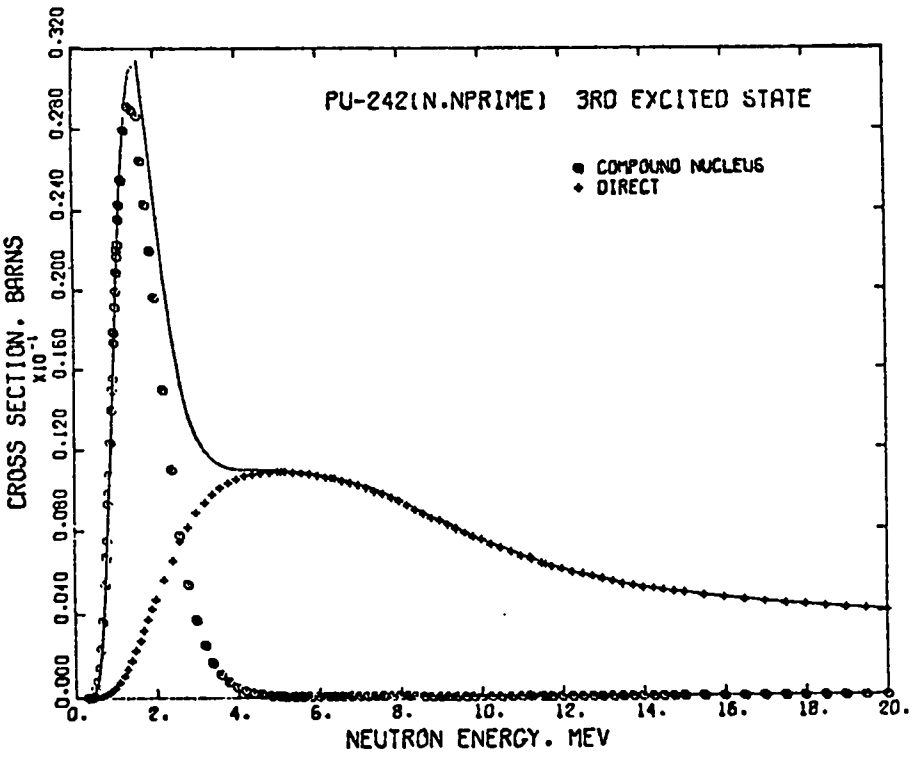

Fig. 6.
Calculated compound nucleus, direct, and total inelastic cross section to the third excited state of ^{242}Pu.

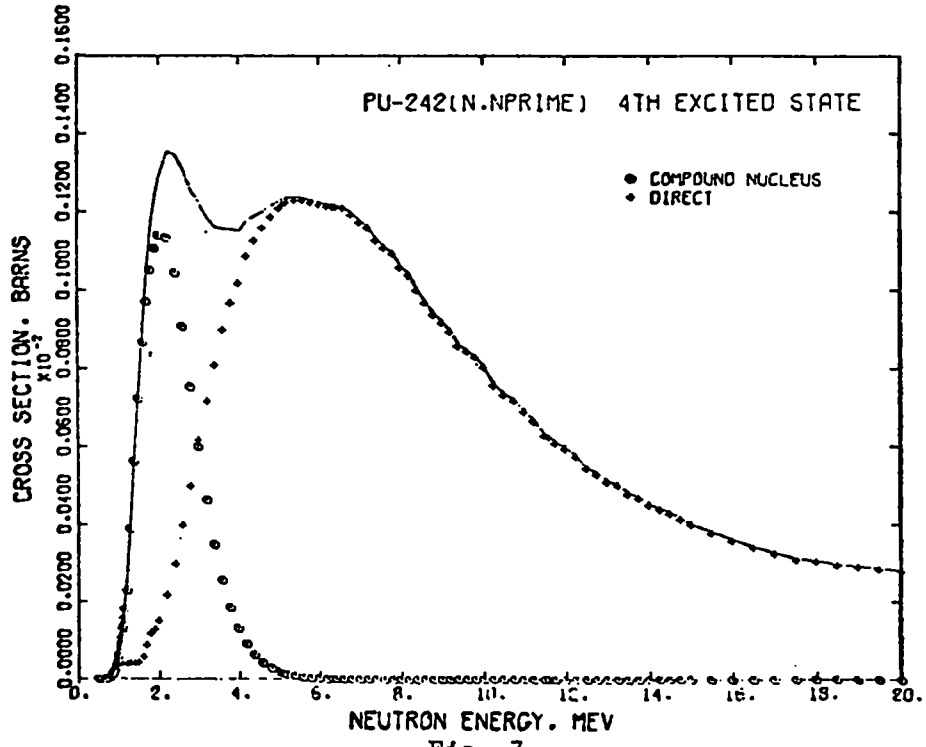

Fig. 7.
Calculated compound nucleus, direct, and total inelastic cross section to the fourth excited state of ^{242}Pu.

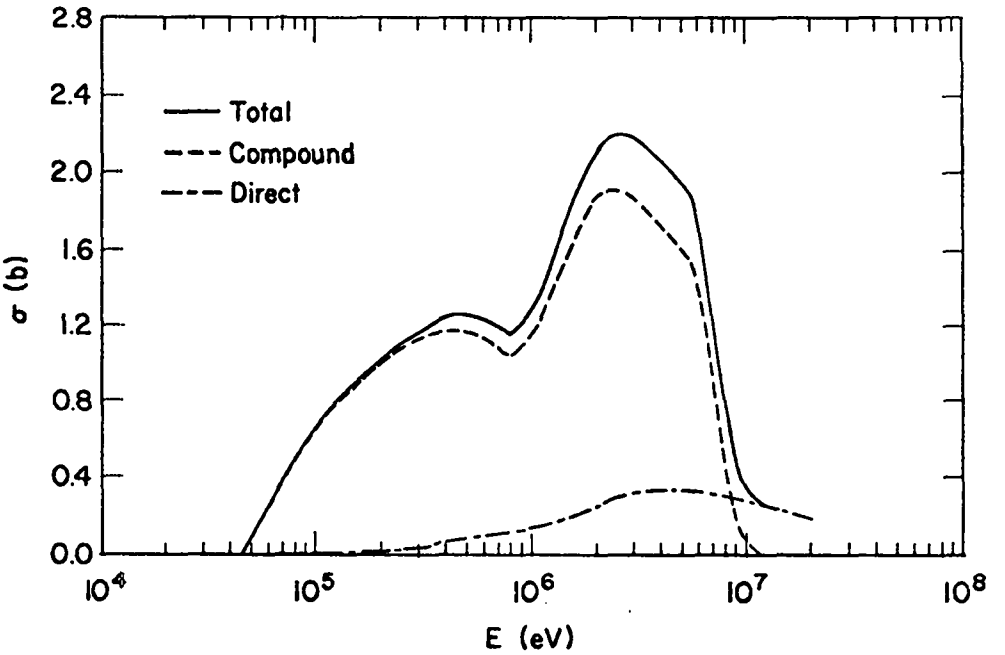

Fig. 8.
Calculated total inelastic scattering for n + ^{242}Pu together with the total compound and total direct inelastic components.

C. Compound-Nucleus Reaction Hauser-Feshbach Calculations.

The compound-nucleus reaction calculations were performed with the LASL version of the code COMNUC[9] (3/29/78 version). This version has the following changes:

1. Non-physical integration ranges have been deleted from the continuum fission calculation for first-, second-, and third-chance fission. Discrete fission channels, up to a maximum of ten, have been introduced into the second- and third-chance fission calculations.[10]
2. A subroutine[11] has been introduced by which discrete level densities are smoothly joined to the Gilbert and Cameron[12] continuous level density expression. The parameters of the constant temperature formula and the matching energy to the Fermi gas expression are adjusted to maintain continuity for the total level density.
3. The branching ratio expressions in the subroutine NCASC have been modified based upon the calculations of Ref. 10.

Calculations were performed for the (n,n'), (n,2n), (n,3n), (n,f), (n,nf), (n,2nf) and (n,γ) reactions. The potential of Table I was used to generate all neutron transmission coefficients for these calculations. Discrete levels were included for the various channels wherever possible. The actual level data used

are summarized in Tables III-VI[13,14] for the nuclei $^{240-243}$Pu, respectively. In instances of unknown spins and parities, assignments were made based upon systematics wherever possible. For the discrete (n,n') calculation, 19 excited levels (Table V) were used up to an excitation of 1.1522 MeV, after which the continuum (n,n') calculation was begun. For the (n,2n) calculation, 10 discrete levels (Table IV) were used up to an excitation of 0.235 MeV; and for the (n,3n) calculation, 10 discrete levels (Table III) were used up to an excitation of 0.900 MeV.

The Gilbert and Cameron[12] level density expression for deformed nuclei was used throughout. In this formulation, the deformed nucleus level density parameter a is given by

$$a = \left[0.12 + 9.17 \times 10^{-3}(SZ + SN)\right] A \quad (MeV^{-1}) \quad , \qquad (2)$$

where the shell correction terms SZ and SN are those of Cook et al.[15] The level density parameters are given in Table VII, where E_0 and T are the constant temperature formula parameters, E_m is the matching energy, and a [Eq. (2)] and δ (pairing energy) characterize the Fermi gas expression. Note that E_0, T, and E_m have been adjusted to smoothly match the discrete level data for ^{242}Pu, ^{241}Pu, and ^{240}Pu, which are formed in the (n,n'), (n,2n), and (n,3n) reactions, respectively.

The (n,f), (n,nf), and (n,2nf) reactions were calculated using the Hill-Wheeler[16] approach with single-hump, one-dimensional, fission barriers. Both discrete and continuum fission channels were employed for first-, second-, and third-chance fission. Initial values of the fission parameters were based upon the results of Back et al.[17,18] for the second (outer) barrier, and these were optimized by fitting to the total fission cross-section data of Auchampaugh et al.[19] and Behrens et al.[20] (see Sec. III.B.) The final set of parameters is given in Table VIII, in which B_n is the neutron binding energy in the compound system, E_B is the barrier height, $\hbar\omega$ is the curvature, $\hbar^2/2I$ is the inertial parameter used in the continuum fission region, N is the number of discrete fission channels, E_c is the excitation energy relative to the barrier at which the continuum fission calculation begins, and AFACT is the enhancement factor of the level density parameter a due to the higher density of compound-nucleus states in the vicinity of the barrier. The discrete fission channels are those of

TABLE III

NUCLEAR LEVEL DATA FOR ^{240}Pu

Level	J^{π}	Excitation (MeV)
1	0^+	0.000
2	2^+	0.0428
3	4^+	0.1417
4	6^+	0.294
5	8^+	0.498
6	1^-	0.597
7	3^-	0.649
8	5^-	0.7422
9	0^+	0.861
10	2^+	0.900

TABLE IV

NUCLEAR LEVEL DATA FOR ^{241}Pu

Level	J^{π}	Excitation (MeV)
1	$5/2^+$	0.000
2	$7/2^+$	0.041
3	?	0.063
4	?	0.067
5	$9/2^+$	0.094
6	$1/2^+$	0.161
7	$3/2^+$	0.170
8	$7/2^+$	0.174
9	$9/2^+$	0.229
10	$(5/2^+)$	0.235

TABLE V

NUCLEAR LEVEL DATA FOR ^{242}Pu

Level	J^{π}	Excitation (MeV)
1	0^+	0.000
2	2^+	0.04454
3	4^+	0.1472
4	6^+	0.3059
5	8^+	0.5176
6	10^+	0.7787
7	1^-	0.7803
8	3^-	0.8329
9	?	0.865
10	(5^-)	0.927
11	0^+	0.956
12	(2^-)	0.9856
13	2^+	0.995
14	3^-	1.0194
15	?	1.0396
16	4^-	1.0640
17	12^+	1.0867
18	(2^+)	1.102
19	(5^-)	1.122
20	(2^-)	1.1522

Tables IV-VI, except that the excitation energies were compressed by a factor 2 based upon the work of Gardner[21] (no attempts were made to reorder the states). Note, however, that discrete fission channel and continuum level densitities were smoothly matched in the manner described above.

The final fit to the total fission cross section is compared to the available measurements[19,20,22-25] in Fig. 9. The calculation agrees to within $\pm$ 5% with the data of Behrens et al.,[20] which were emphasized in the evaluation (see Sec. III.B).

TABLE VI

NUCLEAR LEVEL DATA FOR ^{243}Pu

Level	J^{π}	Excitation (MeV)
1	$7/2^+$	0.000
2	$9/2^+$	0.0579
3	$11/2^+$	0.1244
4	$(13/2^+)$	0.2044
5	$5/2^+$	0.2875
6	$7/2^+$	0.3332
7	$(1/2^+)$	0.3837
8	$(9/2^+)$	0.392
9	$(3/2^+)$	0.3925
10	$9/2^-$	0.4025
11	$(5/2^+)$	0.4468
12	$7/2^+$	0.4501

TABLE VII

LEVEL DENSITY PARAMETERS

Compound Nucleus	E_0 (MeV)	T (MeV)	Em (MeV)	a (MeV^{-1})	δ (MeV)
^{243}Pu	-0.511	0.401	3.827	27.623	0.710
^{242}Pu	-0.015	0.390	4.035	27.797	1.100
^{241}Pu	-0.676	0.395	3.512	27.660	0.490
^{240}Pu	0.020	0.382	3.654	27.083	0.970

TABLE VIII

^{242}Pu FISSION CHANNEL PARAMETERS

	(n,f)	(n,nf)	(n,2nf)
B_n (MeV)	5.037	6.310	5.240
E_B (MeV)	5.39	5.50	5.70
$\hbar\omega$ (MeV)	0.35	0.40	0.40
$\hbar^2/2I$ (keV^{-1})	6.3	7.3	5.8
N	12	10	10
E_c (MeV)	0.225	0.480	0.120
AFACT	1.175	1.05	1.05

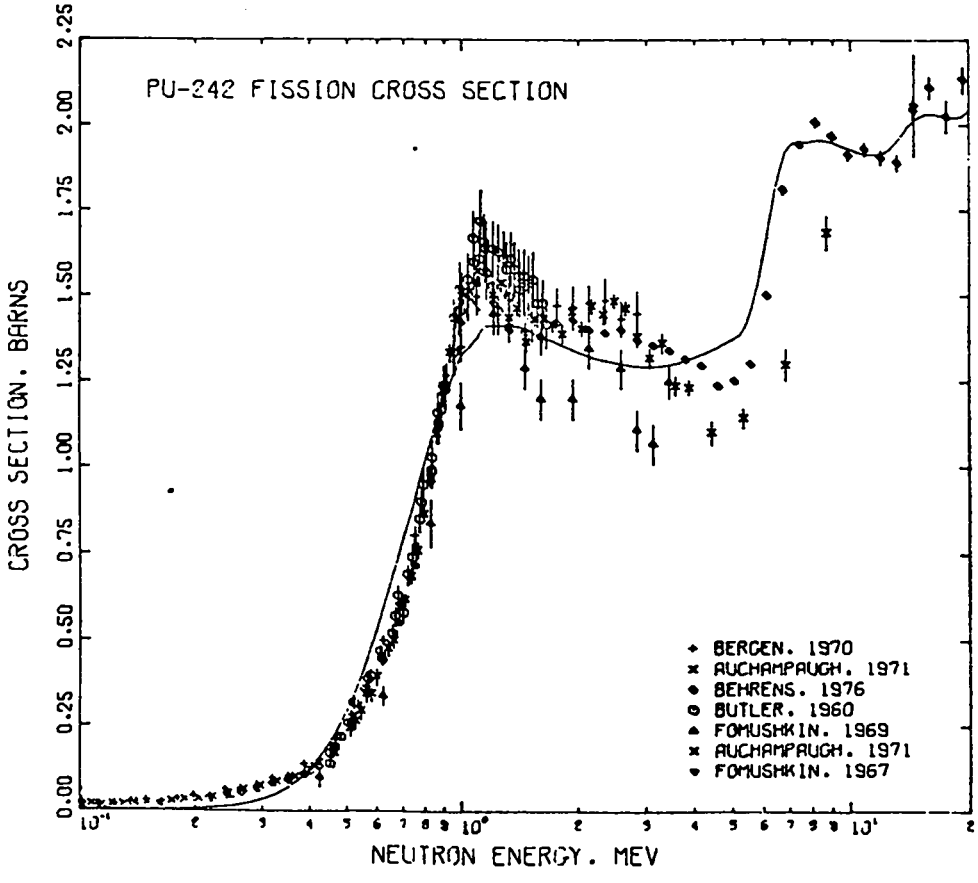

Fig. 9.
Calculated and measured ^{242}Pu(n,f) cross sections above 100 keV.

It is important to note that the calculated total fission cross section is very sensitive to the fission barrier heights. This is illustrated in Fig. 10 where a ∿30% change occurs in the cross section for an ∿6% change in the first-chance fission barrier height. This, of course, strongly affects other open channels. For example, the effect upon the total compound inelastic scattering is shown in Fig. 11.

The ^{242}Pu radiative capture cross section was calculated at all neutron energies using the high-energy approximation in the COMNUC code, that is, only emitted gamma rays with energies greater than the incident neutron energy are assumed to lead to capture. Dipole radiation was assumed in all the calculations. The normalizing value of $2\pi\langle\Gamma_\gamma\rangle/\langle D\rangle$ was obtained by matching the calculated (n,γ) cross section to the measurements of Hockenbury et al.[26] subject to the constraint that $\langle\Gamma_\gamma\rangle$ and $\langle D\rangle$ remain consistent with experimental values and quoted errors[27] (see Table IX). For neutron energies above 4 MeV, a semi-direct contribution was added to the compound-nucleus calculation. The semi-direct component was calculated using a pre-equilibrium cascade process with gamma-ray emission probabilities computed at each stage. Normalization for the calculation was optimized with respect to high-energy capture data for $56 \leq A \leq 238$.[28]

To calculate the (n,2n) and (n,3n) cross sections, it was necessary to determine branching ratios for the competition between neutron emission and fission. This branching was calculated in the manner described in Ref. 9; that is, a neutron cascade model was used to calculate explicitly the competition between the (n,2n), (n,3n), (n,nf), and (n,2nf) reactions. The calculations involved discrete and continuum components, as previously described.

III. EVALUATED CROSS SECTIONS

In this section, the results of the evaluation are presented and compared to the available experimental data. In addition, comparisons are given between the present evaluation (labeled LASL-78) and a recent preliminary evaluation by Mann and Schenter[1] (labeled HEDL-78), a 1976 evaluation by Howerton[29] (labeled LLL-76), and the ENDF/B-IV evaluation by Alter and Dunford[30] (labeled ENDF/B-4).

A. ^{242}Pu(n,γ) Cross Section.

Two separate measurements exist for the ^{242}Pu(n,γ) reaction. The first is that of Hockenbury et al.[26] (1975) in which 15 group-averaged capture data points

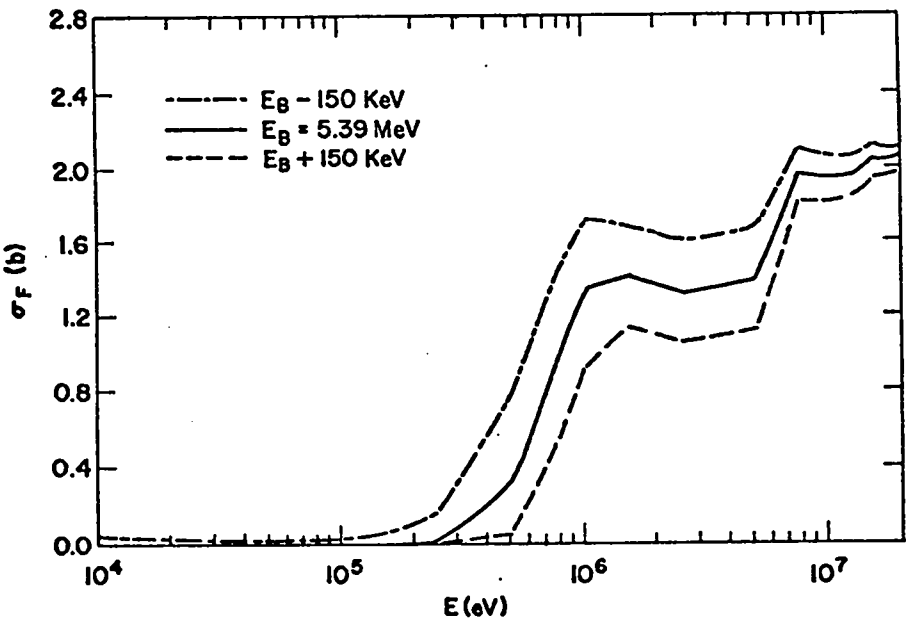

Fig. 10.
Calculated ^{242}Pu(n,f) cross section for three different first-chance fission barrier heights.

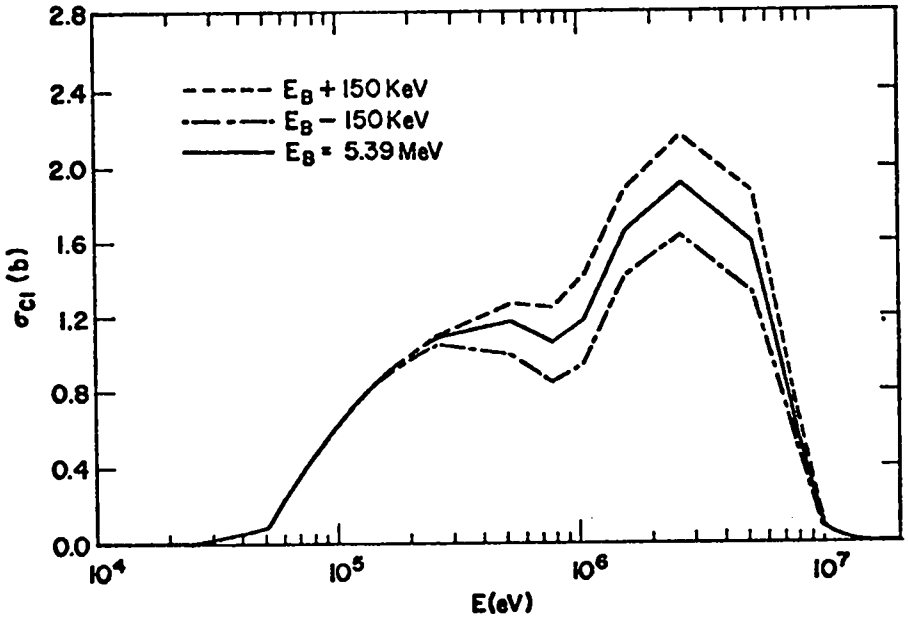

Fig. 11.
Calculated total compound inelastic cross sections corresponding to the three different ^{242}Pu calculations of Fig. 10.

TABLE IX

AVERAGE RADIATIVE WIDTHS AND LEVEL SPACINGS FOR Pu ISOTOPES

Compound Nucleus	$\langle\Gamma_\gamma\rangle$ (meV)	$\langle D\rangle$ (eV)
^{243}Pu	23.5±3	16.5±0.5
^{242}Pu	33.5±8	1.0±0.1
^{241}Pu	31.4±3	13.6±0.4
^{240}Pu	39.8±5	2.3±0.1

were determined covering the range 6 to 70 keV. The overall statistical uncertainty achieved using 2- and 10-keV bin widths is given as ± 4%. The second measurement is that of Wisshak and Käppeler[31] (1978) in which 62 capture data points are reported spanning the energy range 10.4 to 88.9 keV. The estimated total uncertainty in the measurements ranges from ± 6 to ± 10%.

The evaluated (n,γ) cross section is based on the calculation described in Sec. II.C. The experimental data of Hockenbury et al. and Wisshak and Käppeler are compared to the calculated curve and to ENDF/B-IV below 100 keV in Fig. 12. The Hockenbury data, which were used in normalizing the (n,γ) calculation, are in good agreement with the more recent Wisshak measurement.

The (n,γ) cross section over the complete energy range of 0.01-20 MeV is compared in Fig. 13 to the HEDL-78, ENDL-76, and ENDF/B-4 evaluations. Large differences among the evaluations are apparent, particularly above 3 MeV. A value of $\sigma_{n,\gamma} \approx 1$ mb near 14 MeV is supported by recent ^{238}U(n,γ) measurements at LASL.[32]

B. ^{242}Pu(n,f) Cross Section and Spectra.

Six experiments have been reported for the measurement of the ^{242}Pu(n,f) reaction[19,20,22-25] (1959-1978). Two of the measurements were chosen for use in the present evaluation. The 1971 data of Auchampaugh et al.[19] were used to evaluate the low-energy region (10-100 keV) where no other experimental data exist, and the extensive ^{242}Pu/^{235}U fission ratio measurements of Behrens et al.[20] (1978) were used to determine the fission cross section from 100 keV to 20 MeV.

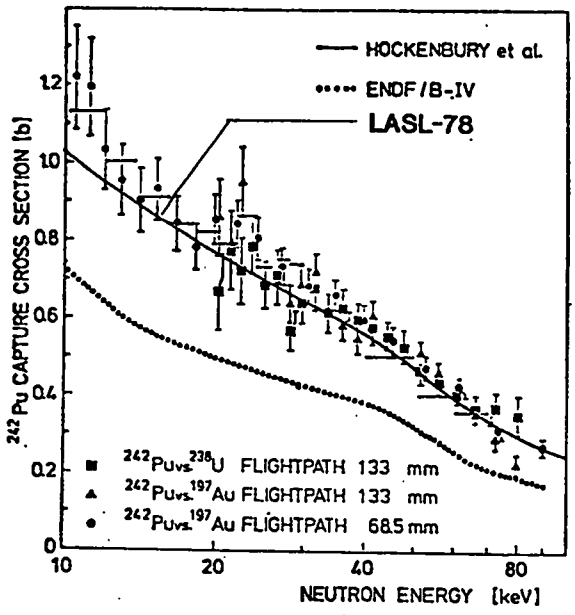

Fig. 12.
Evaluated and measured ^{242}Pu(n,γ) cross section from 10 to 100 keV. The points are from Ref. 31.

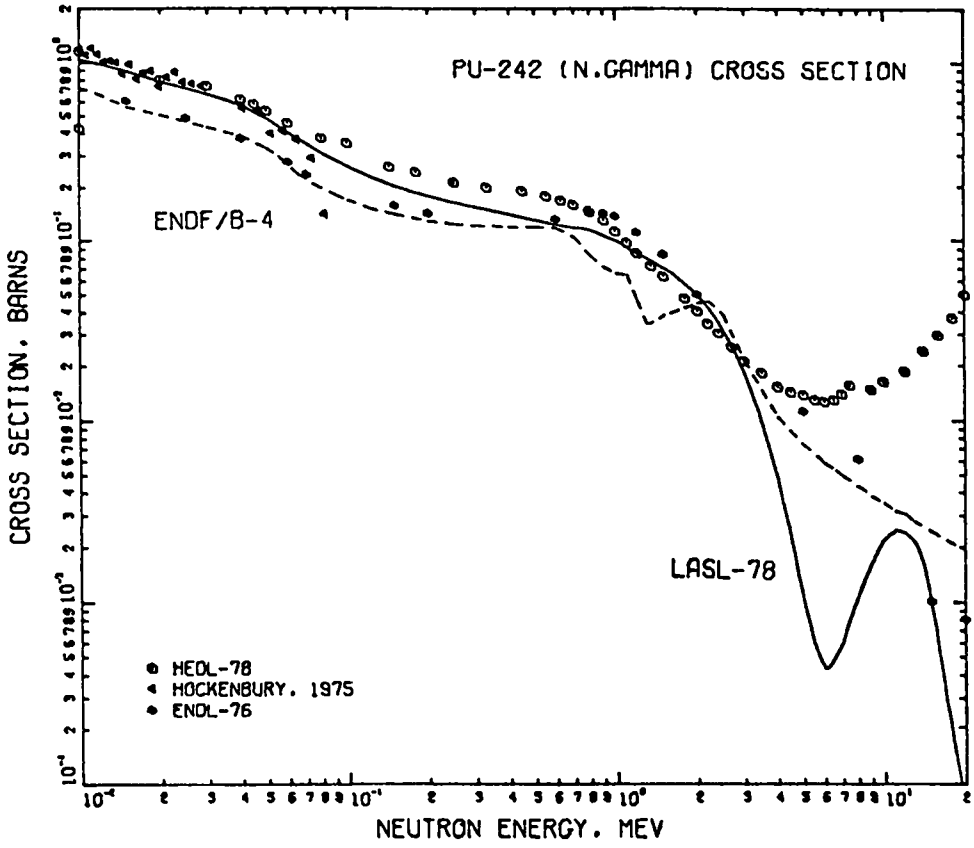

Fig. 13.
Evaluated ^{242}Pu(n,γ) cross sections from 10 keV to 20 MeV. The experimental data of Hockenbury[26] are included.

The fission cross-section data of Auchampaugh et al. were obtained using a nuclear explosion as a neutron source. Auchampaugh's low-energy data were measured relative to the $^{6}Li(n,t)^{4}He$ reaction and normalized using the $^{6}Li(n,\alpha)^{3}H$ data of Schwartz.[33] The overall statistical uncertainty for the data is less than $\pm$ 15% (extracted from Fig. 3 of Ref. 19).

In the measurement of Behrens et al., the ratio of the ^{242}Pu and ^{235}U fission cross sections was obtained for neutron energies between 0.1 and 30 MeV. The experiment was performed at the Lawrence Livermore Electron Linac using time-of-flight techniques and fission ionization chambers. The uncertainty in the neutron energy was $\pm$ 3.5 keV at 1 MeV and $\pm$ 0.31 MeV at 20 MeV. The total rms error in the ^{242}Pu:^{235}U ratio measurements ranges from $\pm$ 1.8 to $\pm$ 18.2%, but averages to $\pm$ 2.8% over the total energy range. For the present analysis, the ENDF/B-V evaluation of the ^{235}U fission cross section[34] was used to convert the Behrens ratio measurements to absolute ^{242}Pu fission cross sections.

The evaluated results are compared to the experimental data in Figs. 14 and 15. Note that the Auchampaugh data were averaged in coarse energy bins before constructing the curve shown in Fig. 14 for the region below 100 keV and that the experimental data in Fig. 15 show considerable dispersion above 1 MeV. The Behrens ratio experiment was adopted for the present evaluation because ratios for other actinides in the same measurement series yield fission cross sections in good agreement with accepted values, it spans almost the total energy range of interest, and it is the most recent measurement.

Different evaluations of the ^{242}Pu fission cross section are compared in Figs. 16 and 17. The HEDL-78 and ENDL-76 evaluations are similar to the present evaluation, since they are also based upon the Behrens experiment. The most significant difference occurs for the ENDF/B-IV evaluation, which is substantially higher than the other data sets below 200 keV and between 2 and 8 MeV.

The evaluated fission spectrum was assumed to follow a Maxwellian distribution

$$N(E'_n) \propto \sqrt{E'_n}\ \exp(-E'_n/T) \quad , \tag{3}$$

where E'_n is the emitted neutron energy. The nuclear temperature T is related to the average number of prompt neutrons emitted per fission $\bar{\nu}_p$, as follows:[35]

$$T(E_n) = 0.50 + 0.43\sqrt{\bar{\nu}_p(E_n) + 1} \quad , \tag{4}$$

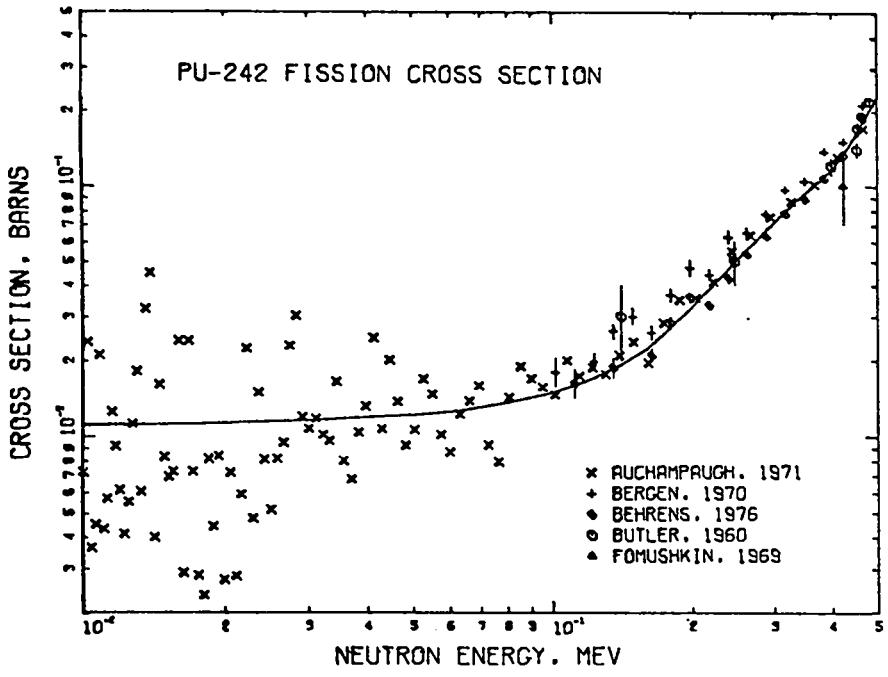

Fig. 14.
Experimental and evaluated $^{242}Pu(n,f)$ cross sections between 10 and 50 keV. The solid curve is the LASL-78 evaluation.

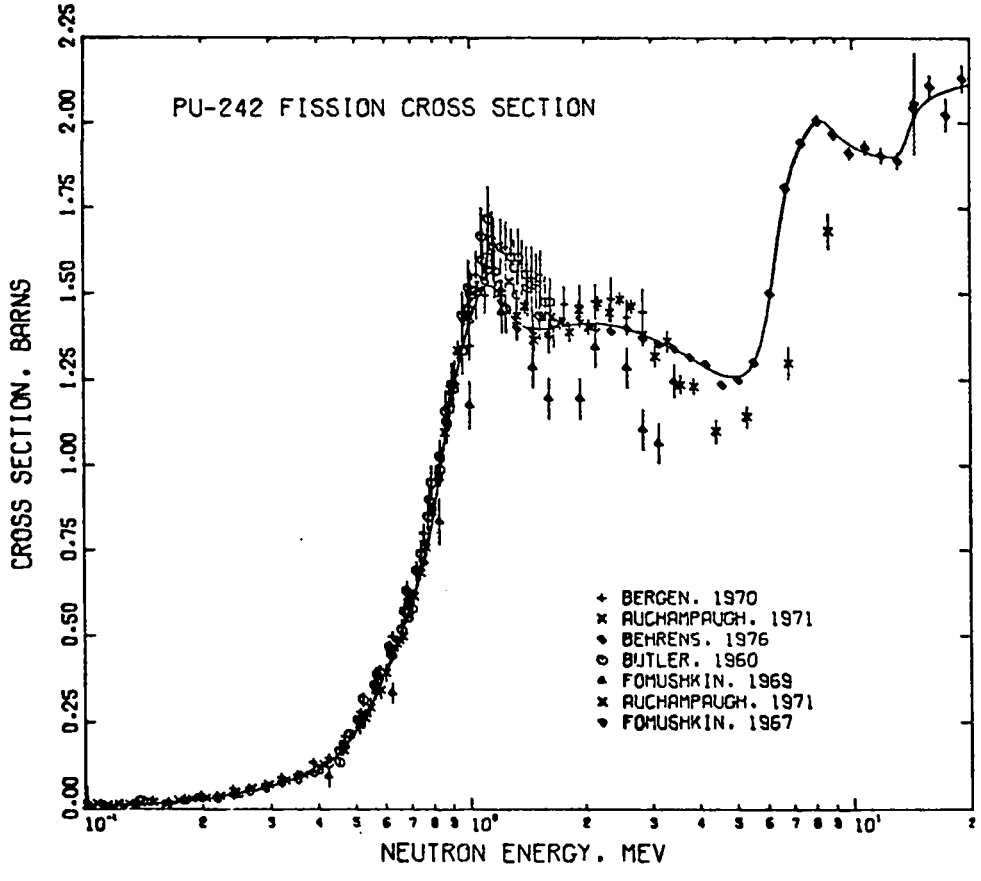

Fig. 15.
Experimental and evaluated $^{242}Pu(n,f)$ cross sections between 0.1 and 20 MeV. The solid curve is the LASL-78 evaluation.

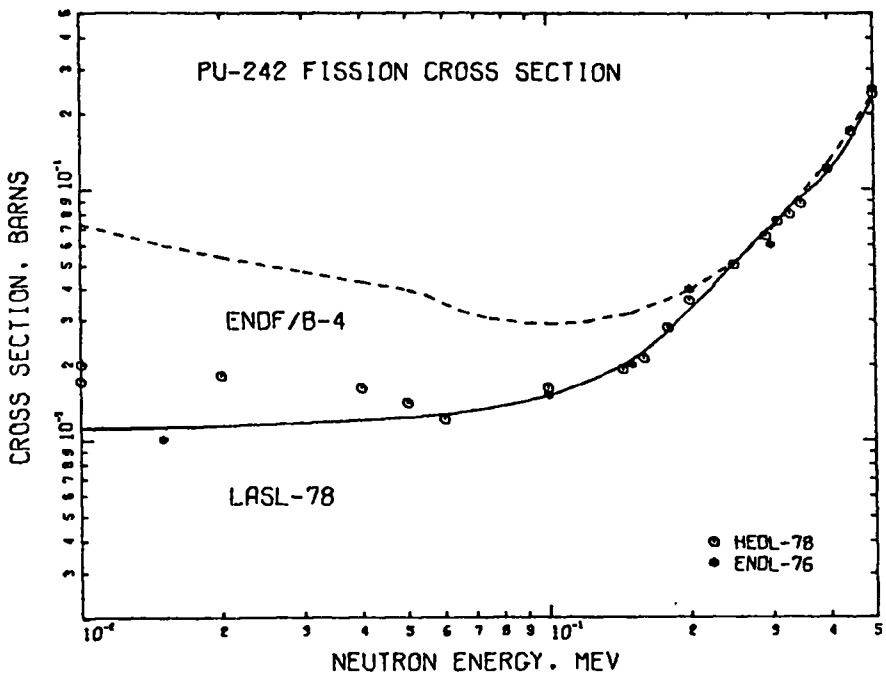

Fig. 16.
Evaluated $^{242}Pu(n,f)$ cross sections from 10 to 500 keV.

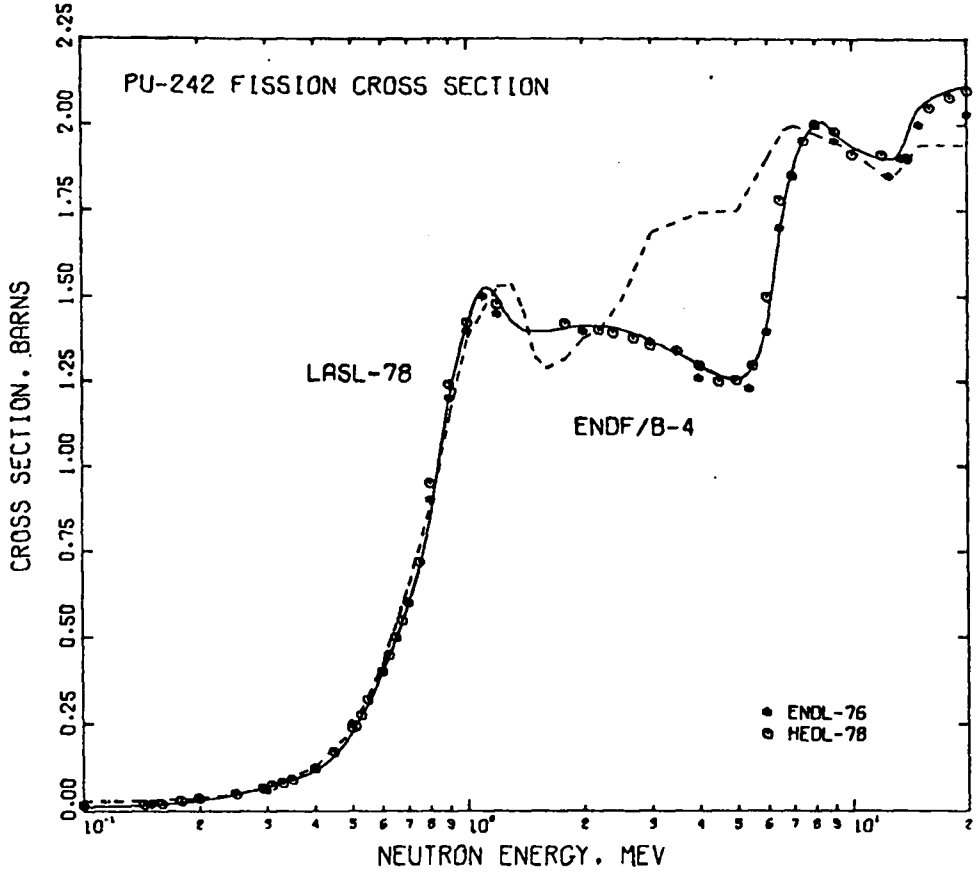

Fig. 17.
Evaluated $^{242}Pu(n,f)$ cross sections from 0.1 to 20 MeV.

where E_n is the incident neutron energy. With this representation, the average energy of fission neutrons induced by 1-MeV incident neutrons is 2.031 MeV.

C. Average Number of Neutrons Emitted Per Fission ($\bar{\nu}$)

There were no ^{242}Pu experimental data available for the determination of $\bar{\nu}_p$, the average number of prompt neutrons emitted per fission. To determine $\bar{\nu}_p$, the substantial experimental data available for the case of neutrons incident on ^{240}Pu were analyzed, and the results were corrected to ^{242}Pu using observations of the systematic variation of $\bar{\nu}_p$ with mass number.

The $\bar{\nu}_p$ expression for ^{240}Pu was taken from the results of Bois and Frehaut[36] and corrected to the ENDF/B-V standard of $\bar{\nu}_p(^{252}\text{Cf}) = 3.757$, which yielded

$$\bar{\nu}_p(^{240}\text{Pu}) = 2.815 + 0.1514\ E_n \quad . \tag{5}$$

Corrections to Eq. (5) for the additional two neutrons present in ^{242}Pu were made using Eq. (4) of Ref. 36, resulting in the expression

$$\bar{\nu}_p(^{242}\text{Pu}) = 2.795 + 0.1576\ E_n \quad . \tag{6}$$

The solid curve in Fig. 18 compares the ^{240}Pu $\bar{\nu}_p$ result [Eq. (5)] with the experimental data of Frehaut et al.[37] and DeVroey et al.;[38] the dashed curve shows the ^{242}Pu result from Eq. (6).

A comparison of the different evaluations of $\bar{\nu}_p(E_n)$ is given in Fig. 19. Below 6 MeV, the LASL-78, ENDL-76, and ENDF/B-IV evaluations are in good agreement, whereas the HEDL-78 values, which are based upon a phenomenological model by Manero and Koshin,[39] are 3-4% higher than the other data. While this difference is small, the higher values are not consistent with other representations of $\bar{\nu}_p$ systematics.[36,40]

A value of 0.015 was adopted for the average number of delayed neutrons emitted per fission $\bar{\nu}_d$. This result was taken from the experimental data of Krick and Evans,[41] as tabulated in the review article of Manero and Konshin.[39] Because no information is available on the energy dependence of $\bar{\nu}_d$ for ^{242}Pu, we assumed it constant. The expression for total $\bar{\nu}$ that results is

$$\bar{\nu}_t(^{242}\text{Pu}) = 2.810 + 0.1576\ E_n \quad . \tag{7}$$

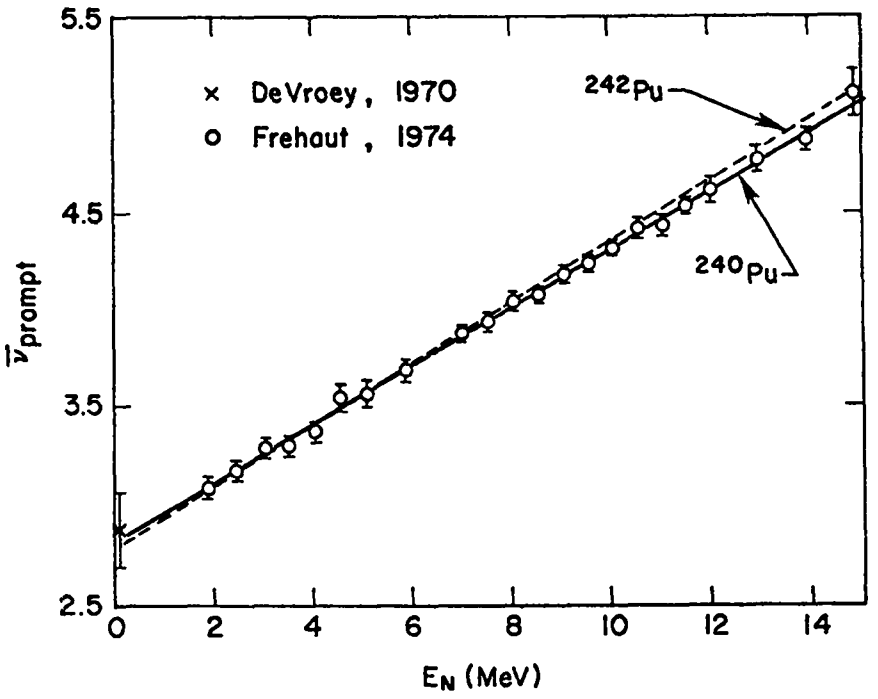

Fig. 18.
Experimental data for $\bar{\nu}_p$ (^{240}Pu) compared to evaluated curves for ^{240}Pu (solid curve) and ^{242}Pu (dashed curve). See text for details.

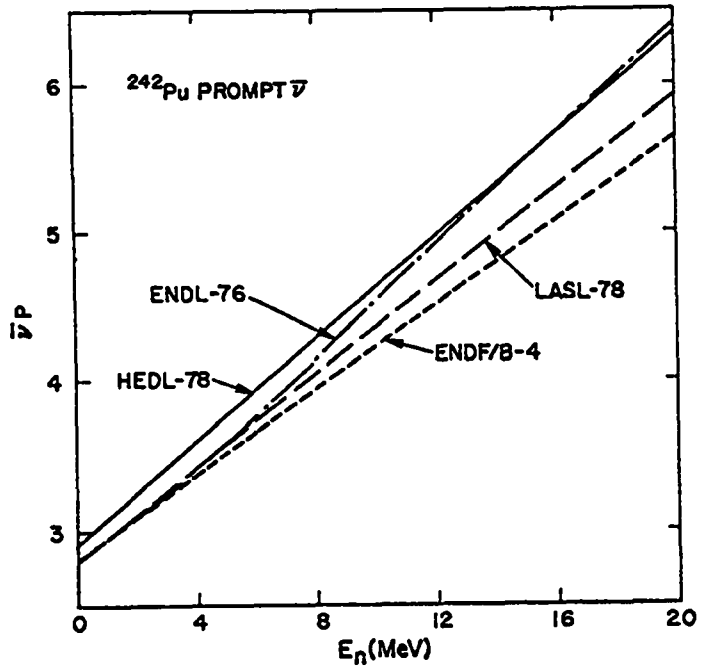

Fig. 19.
Four evaluations of $\bar{\nu}_p$(^{242}Pu) for neutron energies between 0 and 20 MeV.

D. ^{242}Pu(n,n') Cross Sections, Angular Distributions, and Spectra.

The evaluated inelastic scattering cross sections are taken directly from the calculations described in Secs. II.B and II.C. Discrete inelastic data are included for the 19 lowest known excited levels of ^{242}Pu. The excitation cross sections for the first four levels include direct and compound-nucleus components (see Figs. 4-7); the data for the remaining levels are based on compound-nucleus calculations alone. Angular distributions, based on direct and compound-nucleus reaction calculations, are included for the three lowest excited levels.

Inelastic scattering to levels above an excitation energy of 1.152 MeV are lumped into a continuum cross section. [A second (small) continuum component was also included to account for the calculated (n,γn') cross section.] The energy distribution of the continuum neutrons is represented by an evaporation spectrum

$$N(E'_n) \propto E'_n \exp(-E'_n/T) \quad , \tag{8}$$

where E'_n is the secondary neutron energy.

The nuclear temperature T was inferred from the Fermi gas level density parameter a used in the Hauser-Feshbach calculations by matching the slopes of the constant nuclear temperature and Fermi gas level density expressions[12] at an excitation energy equal to the incident neutron bombarding energy E_n resulting in the expression

$$1/T\ (E_n) = \sqrt{\frac{a}{E_n - \Delta}} - \frac{1.5}{E_n - \Delta} \quad , \tag{9}$$

where Δ is a pairing correction taken from the work of Cook et al.[15]

The total inelastic cross section is compared to other evaluations in Fig. 20. Numerous differences exist among the data sets; one of the more significant is the fact that the maximum in the ENDL-76 cross section is broader and occurs some 1-3 MeV lower in energy than for the other data sets. The present evaluation lies closest to the ENDF/B-IV curve.

The average emitted neutron energy from inelastic scattering is shown as a function of incident neutron energy in Fig. 21 for incident energies up to 5 MeV. For comparison, values are also included from the ENDF/B-IV ^{238}U evaluation. The ENDL/76 (n,n') spectrum is significantly softer below 1 MeV than the other data

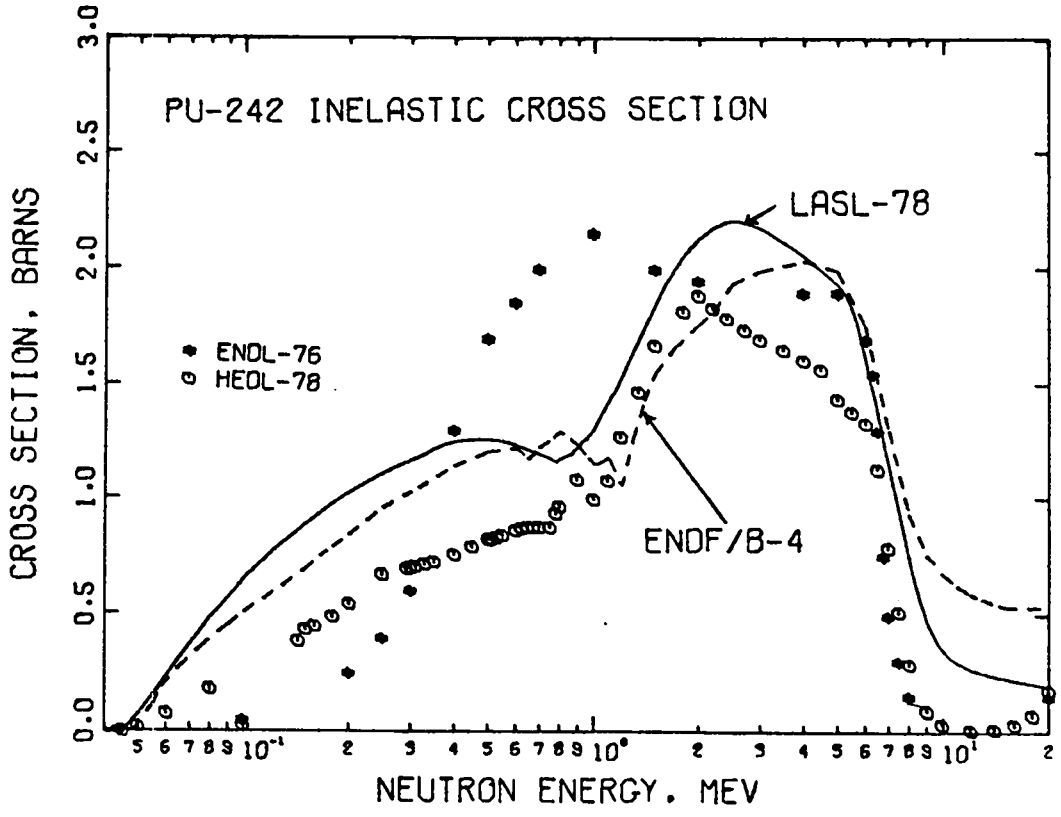

Fig. 20.
Evaluated ^{242}Pu total inelastic cross sections from threshold to 20 MeV.

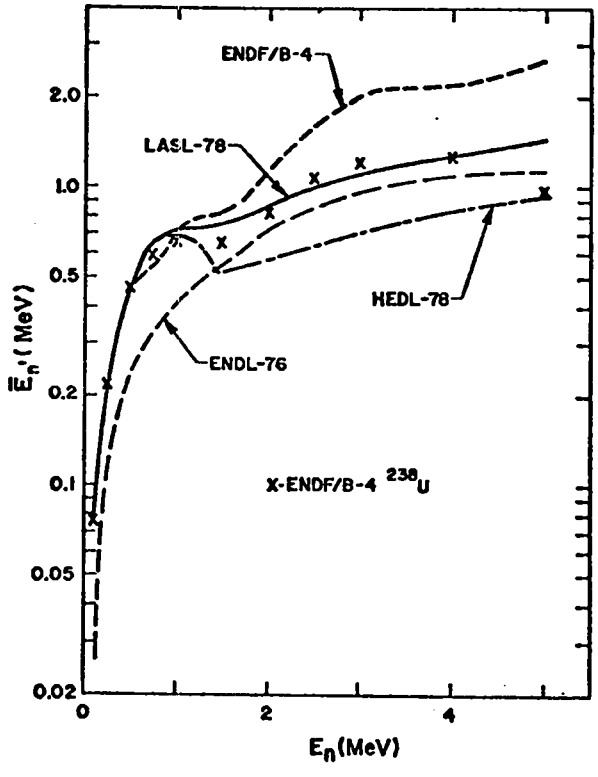

Fig. 21.
The average emitted neutron energy from ^{242}Pu inelastic scattering at incident neutron energies between 0 and 5 MeV. Results are shown for four ^{242}Pu evaluations and for the ENDF/B-IV evaluation of ^{238}U.

sets; at higher energies, significant differences exist among all the evaluations. The present results fall closest to the ^{238}U Version IV evaluation.

Graphs of the neutron energy spectra from (n,n') reactions are shown for the various evaluations in Figs. 22-24 for incident neutron energies of 1.0, 1.5, and 2.5 MeV, respectively. The softness of the ENDL-76 spectrum relative to the other data sets is seen in Fig. 22 to result from the absence of discrete level data in that evaluation. Relatively large differences occur among all the evaluated spectra.

E. $^{242}Pu(n,2n)$ and $^{242}Pu(n,3n)$ Cross Sections and Spectra.

The calculations described in Sec. II.C were used to determine evaluated (n,2n) and (n,3n) cross sections. The results are compared to data from other evaluations in Figs. 25 and 26. Neutron energy distributions from the (n,2n) and (n,3n) reactions are represented as evaporation spectra using Eq. (8). In this case, the nuclear temperatures were calculated from the nuclear level density parameters with the expression

$$1/T\ (E_n) = \sqrt{\frac{a}{E_n + Q - \Delta}} - \frac{1.5}{E_n + Q - \Delta}\ , \qquad (10)$$

where Q is the Q-value for the (n,2n) or (n,3n) reactions and a and Δ have been defined previously.

F. ^{242}Pu Total Cross Section.

The ^{242}Pu total cross section was obtained by combining the calculations of Sec. II in an ad hoc manner. Specifically, the deformation effects (inelastic scattering in the coupled-channels formalism) were combined with the total cross section calculated with the spherical potential of Table I to obtain the deformed nucleus total cross section. This procedure was justified (approximately) by tests on the uranium isotopes where measured total cross section data exist.

The total cross sections from 10 keV to 20 MeV are compared for the four evaluations in Fig. 27. The peak in the ENDL-76 total cross section near 1 MeV results from the peak in the (n,n') cross section shown in Fig. 20.

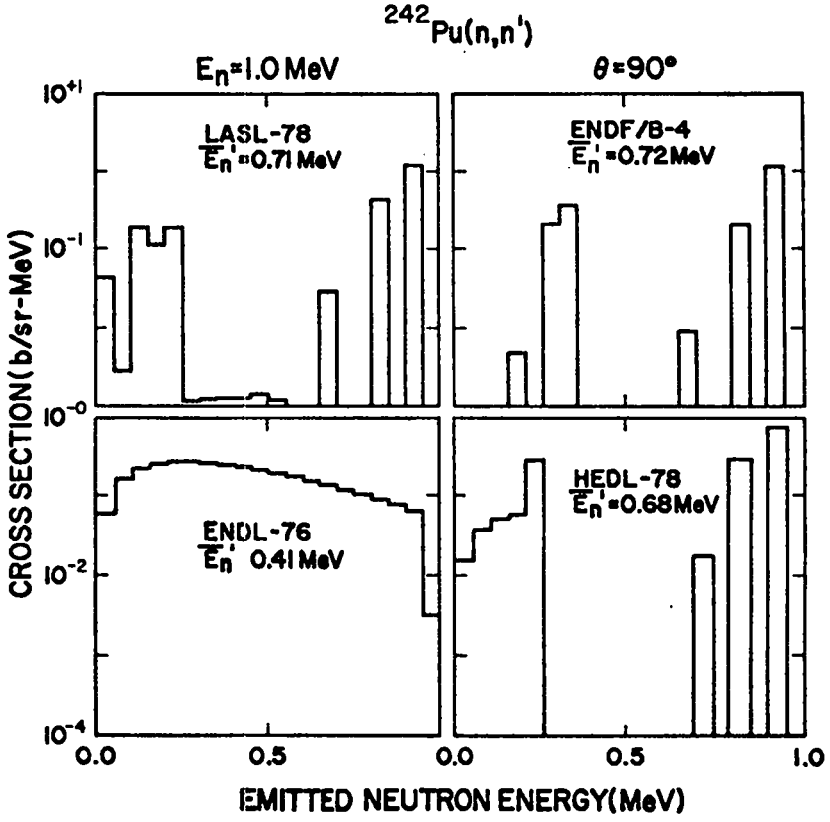

Fig. 22.
Evaluated neutron emission spectra from $^{242}Pu(n,n')$ reactions at an incident energy of 1.0 MeV.

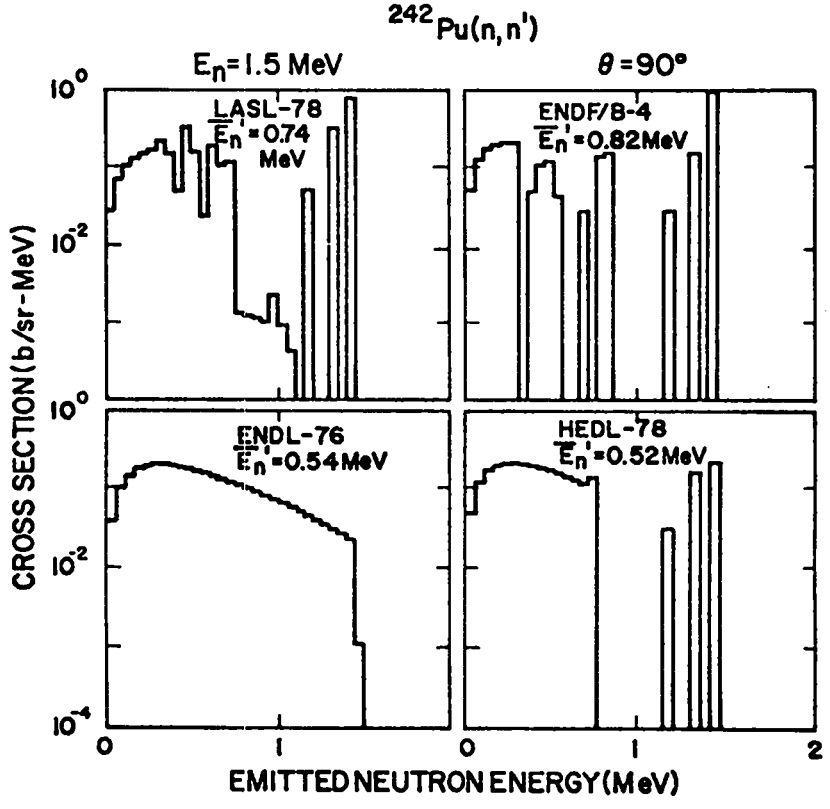

Fig. 23.
Evaluated neutron emission spectra from $^{242}Pu(n,n')$ reactions at an incident energy of 1.5 MeV.

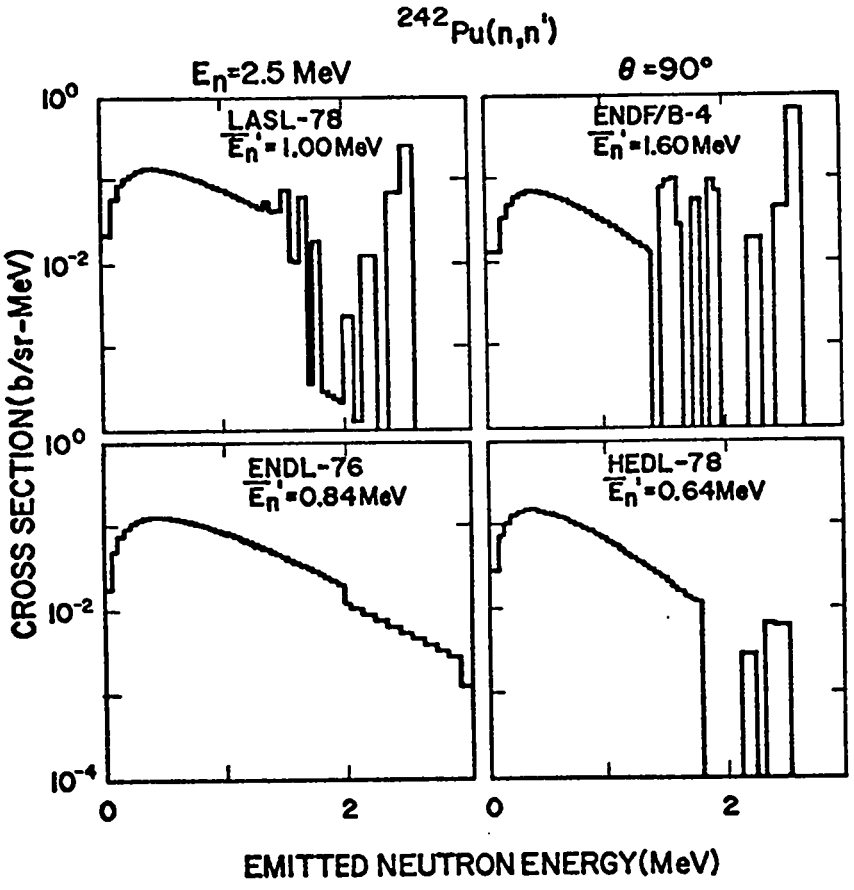

Fig. 24.
Evaluated neutron emission spectra from ^{242}Pu(n,n') reactions at an incident energy of 2.5 MeV.

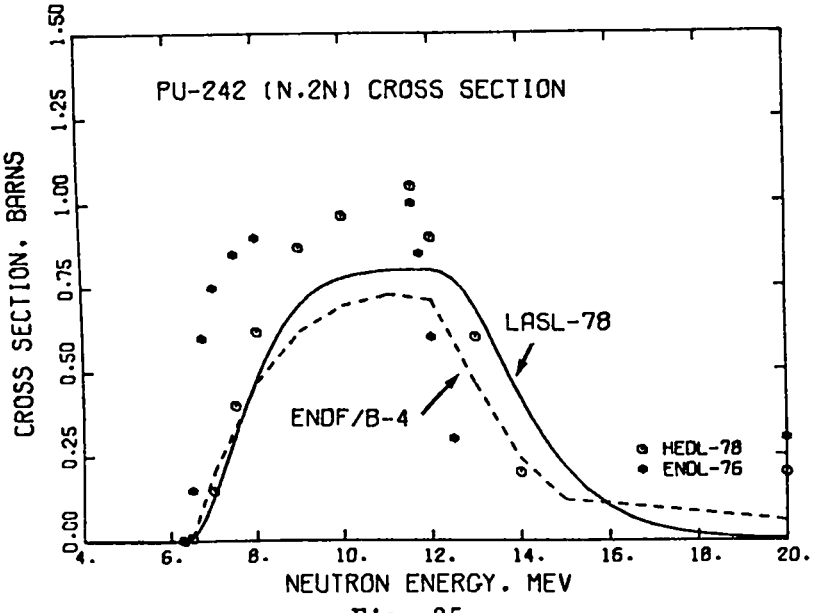

Fig. 25.
Comparisons of evaluated ^{242}Pu(n,2n) cross sections from threshold to 20 MeV.

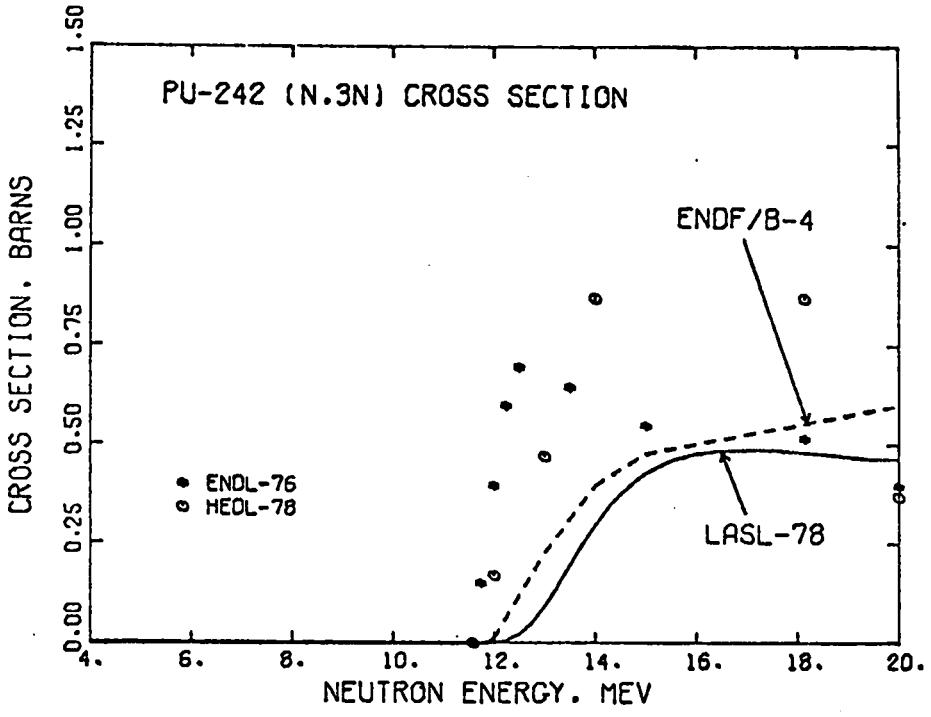

Fig. 26.
Comparisons of evaluated $^{242}Pu(n,3n)$ cross sections from threshold to 20 MeV.

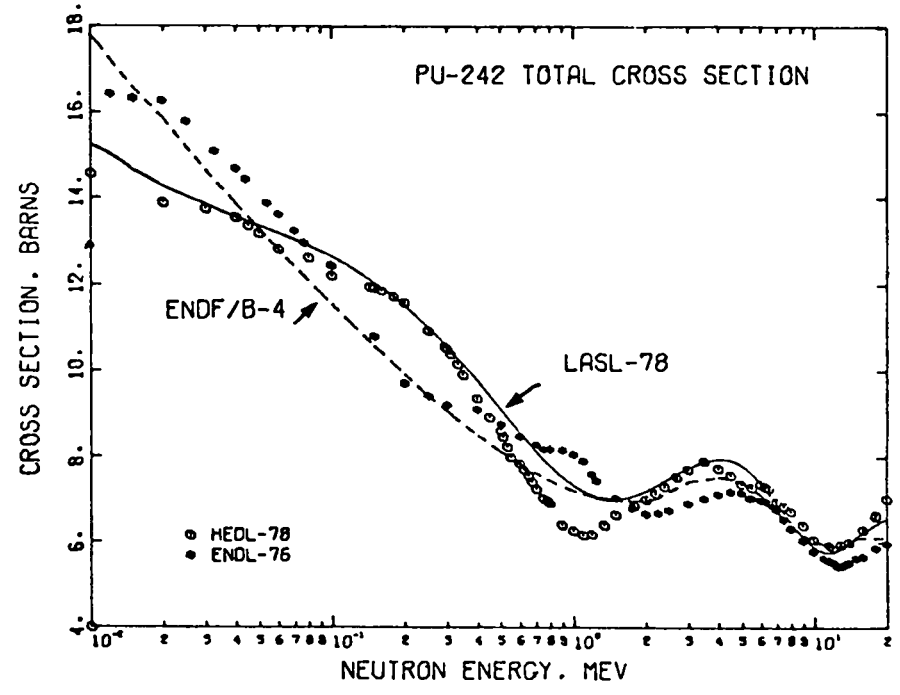

Fig. 27.
Comparisons of evaluated ^{242}Pu total cross sections from 10 keV to 20 MeV.

G. ^{242}Pu Elastic Cross Section and Angular Distributions.

The evaluated elastic cross sections from 0.01 to 20 MeV were obtained by subtracting the sum of the nonelastic cross sections from the total cross section. The evaluated curve differs from the actual elastic scattering calculation of Sec. II by at most $\pm$ 100 mb, due primarily to differences between the calculated and evaluated fission cross sections. The evaluated elastic cross section is shown in Fig. 28 with other evaluated results.

The elastic scattering angular distributions were determined from the compound-nucleus and direct reaction theory calculations of Sec. II. The compound elastic component was assumed isotropic, and the direct component was taken from the JUKARL calculations. A comparison of the elastic angular distributions for 1-MeV incident neutrons is given in Fig. 29 for several evaluations. Similarly, in Fig. 30 the average value of the cosine of the center-of-mass scattering angle is plotted as a function of incident energy (up to 5 MeV) for the various evaluations.

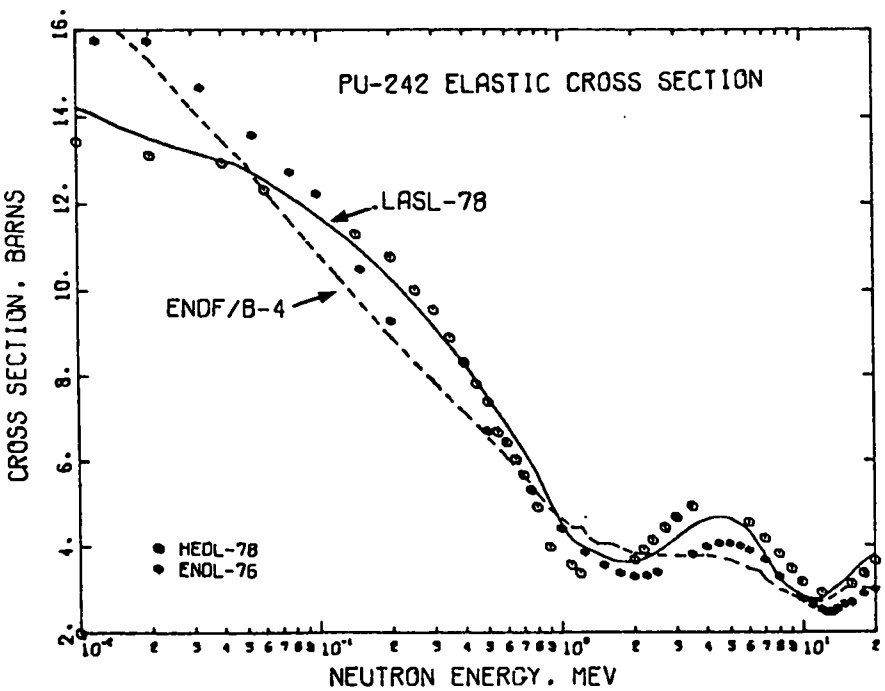

Fig. 28.
Comparisons of evaluated ^{242}Pu elastic cross sections from 10 keV to 20 MeV.

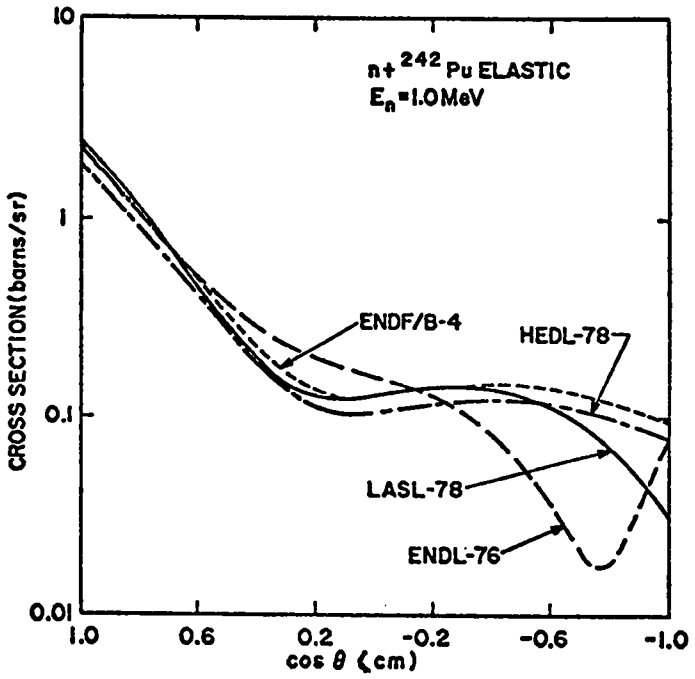

Fig. 29.
Comparisons of evaluated elastic scattering angular distribution for 1-MeV neutrons incident on ^{242}Pu.

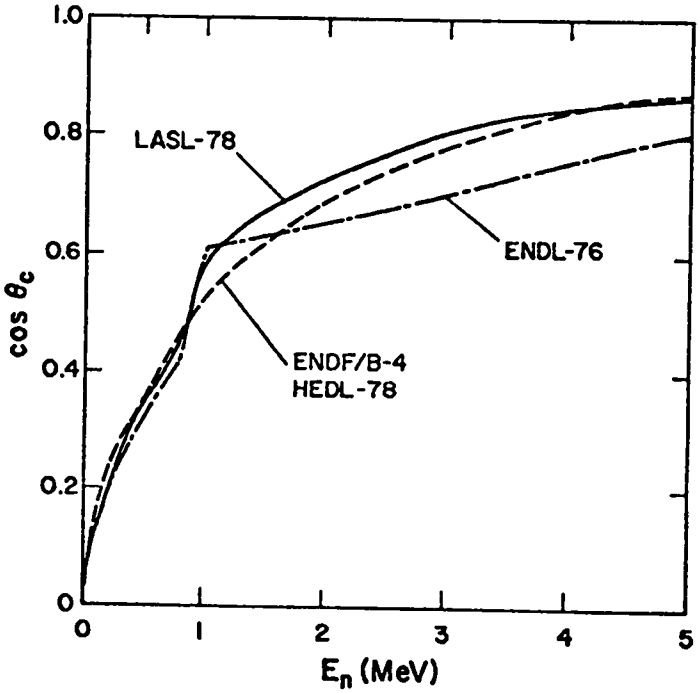

Fig. 30.
The average value of the cosine of the center-of-mass elastic scattering angle for several ^{242}Pu evaluations at incident energies up to 5 MeV.

V. SUMMARY

Because of the sparsity of experimental data, it was necessary to rely upon nuclear model calculations for much of the present evaluation. These calculations are the most extensive yet performed for ^{242}Pu and should provide reasonably reliable estimates of unmeasured ^{242}Pu data. However, because of uncertainties in the calculations, there is a need for new experimental data to validate and improve these results. In particular, measurements of the total, elastic, and inelastic cross sections and angular distributions are needed at neutron energies corresponding to a fission spectrum (few hundred keV to several MeV). The average number of neutrons per fission should be measured for the same range together with a few high-energy points ($\sim$14 MeV). Finally, independent measurements to verify the fission cross sections inferred from the ratio data of Behrens et al.[20] would be very useful, as would a measurement to check the shape of the fission spectrum assumed in the present evaluation. With the addition of these new data, together with the completion of the deformed optical potential (Sec. II.A) and an improved fission channel description (Sec. II.C), a more definitive evaluation could be made.

REFERENCES

1. F. Mann and R. E. Schenter, "HEDL Evaluation of Actinide Cross Sections for ENDF/B-V," Hanford Engineering Development Laboratory report HEDL-TME-77-54 (1977).

2. D. G. Madland, "Neutron Optical Potential for Uranium Isotopes," in "Applied Nuclear Data Research and Development July 1 - September 30, 1977," compiled by C. I. Baxman and P. G. Young, Los Alamos Scientific Laboratory report LA-7066-PR (Dec. 1977).

3. D. Wilmore and P. E. Hodgson, "The Calculation of Neutron Cross Sections from Optical Potentials," Nucl. Phys. 55, 673 (1964).

4. F. D. Becchetti, Jr., and G. W. Greenlees, "Nucleon-Nucleus Optical-Model Parameters, A > 40, E < 50 MeV," Phys. Rev. 182, 1190 (1969).

5. F. G. Perey, "Optical-Model Analysis of Proton Elastic Scattering in the Range 9-22 MeV," Phys. Rev. 131, 745 (1963).

6. D. G. Foster, Jr., and D. W. Glasgow, "Neutron Total Cross Sections, 2.5-15 MeV, I. Experimental," Phys. Rev. C3, 576 (1971).

7. H. Rebel and G. W. Schweimer, "Improved Version of Tamura's Code for Coupled-Channel Calculations: JUPITOR Karlsruhe Version," Gesellschaft fur Kernforschung M.B.H. report KFK.133 (Feb. 1971).

8. C. F. Bemis, F. K. McGowan, J. L. C. Ford, Jr., W. T. Milner, P. H. Stelson, and R. L. Robinson, "E2 and E4 Transition Moments and Equilibrium Deformations in the Actinide Nuclei," Phys. Rev. C8, 1466 (1973).

9. C. L. Dunford, "A Unified Model for Analysis of Compound Nucleus Reactions," Atomics International report AI-AEC-12931 (July 1970).

10. D. G. Gardner, Lawrence Livermore Laboratory, personal communication (January 1978).

11. P. G. Young and E. D. Arthur, "GNASH: A Preequilibrium, Statistical Nuclear-Model Code for Calculation of Cross Sections and Emission Spectra," Los Alamos Scientific Laboratory report LA-6947 (Nov. 1977).

12. A. Gilbert and A. G. W. Cameron, "A Composite Nuclear Level Density Formula with Shell Corrections," Can. J. Phys. 43, 1446 (1965).

13. D. J. Horen, Ed., Nuclear Level Schemes A = 45 through A = 257 from Nuclear Data Sheets (Academic Press, Inc., New York, 1973).

14. Y. A. Ellis and R. L. Haese, "Nuclear Data Sheets for A = 242," Nuclear Data Sheets 21, 615 (1977).

15. J. L. Cook, H. Ferguson, and A. R. DeL. Musgrove, "Nuclear Level Densities in Intermediate and Heavy Nuclei," Aust. J. Phys. 20, 477 (1967).

16. D. L. Hill and J. A. Wheeler, "Nuclear Constitution and the Interpretation of Fission Phenomena," Phys. Rev. 89, 1102 (1953).

17. B. B. Back, Ole Hansen, H. C. Britt, and J. D. Garrett, "Fission of Doubly Even Actinide Nuclei Induced by Direct Reactions," Phys. Rev. C9, 1924 (1974).

18. B. B. Back, H. C. Britt, Ole Hansen, B. Leroux, and J. D. Garrett, "Fission of Odd-A and Double Odd-A Actinide Nuclei Induced by Direct Reactions," Phys. Rev. C10, 1948 (1974).

19. G. F. Auchampaugh, J. A. Farrell, and D. W. Bergen, "Neutron-Induced Fission Cross Sections of ^{242}Pu and ^{244}Pu," Nucl. Phys. A171, 31 (1971).

20. J. W. Behrens, R. S. Newbury, and J. W. Magana, "Measurements of the Neutron-Induced Fission Cross Sections for ^{240}Pu, ^{242}Pu, and ^{244}Pu Relative to ^{235}U from 0.1 to 30 MeV," Nucl. Sci. Eng. 66, 433 (1978).

21. D. G. Gardner, "Neutron Reactions on ^{237}U," Lawrence Livermore Laboratory report UCID-16885 (1975).

22. D. W. Bergen and R. R. Fullwood, "Neutron-Induced Fission Cross Sections of ^{242}Pu," Nucl. Phys. A163, 577 (1971).

23. D. K. Butler, "Neutron-Induced Fission Cross Section of Pu^{242} from 0.1 to 1.5 MeV," Am. Phys. Soc. 4, 234 (1959).

24. E. F. Formushkin, E. K. Futnikova, Yu. S. Zamustrin, B. K. Moslennikov, V. N. Belov, V. M. Surin, F. Nasyrov, and N. F. Paskin, "Cross Sections and Fragment Angular Anisotropy in Fast-Neutron Fission of Some Isotopes of Plutonium, Americium, and Curicum," Yad Fiz. (Sov. J. Nucl. Phys.) 5, 689 (1967).

25. E. F. Formushkin and E. F. Gutnikova, "Cross-Section and Angular Distributions of Fragments in the Fission of ^{238}Pu, ^{242}Pu, and ^{241}Am by Neutrons on Energy of 4.35-3.6 MeV," International Nuclear Data Committee report INDC (CCP)-7/u, p. 28 (1970).

26. R. W. Hockenbury, A. J. Sanislo, and N. N. Kaushal, "KeV Capture Cross Section of ^{242}Pu," in NBS Special Publication 425, Vol. II, p. 584 (National Bureau of Standards, US Department of Commerce, Oct. 1975).

27. S. F. Mughabghab and D. I. Garber, Eds., "Neutron Cross Sections, Vol. 1, Resonance Parameters," Brookhaven National Laboratory report 325 (June 1973).

28. E. D. Arthur, Los Alamos Scientific Laboratory, personal communication (April 1978).

29. R. J. Howerton, D. E. Cullen, R. C. Haight, M. H. MacGregor, S. T. Perkins, and E. F. Plechaty, "The LLL Evaluated Nuclear Data Library, (ENDL) Evaluation Techniques, Reaction Index, and Descriptions of Individual Evaluations," Lawrence Livermore Laboratory report UCRL-50400 Vol. 15 (1975).

30. H. Alter and C. Dunford, Brookhaven National Laboratory, personal communication (1974).

31. K. Wisshak and F. Käppeler, "Neutron Capture Cross-Section Ratios of ^{240}Pu, ^{242}Pu, ^{238}U, and ^{197}Au in the Energy Range from 10 to 90 keV," Nucl. Sci. Eng. 66, 363 (1978).

32. D. Drake, Los Alamos Scientific Laboratory, personal communication (1978).

33. S. Schwartz, L. G. Stromberg, and A. Bergstron, "A Relative Measurement of the $Li^6(n,\alpha)H^3$ Reaction Cross Section in the Range $1 < E_n < 600$ keV," Nucl. Phys. 63, 593 (1965).

34. M. Bhat, Brookhaven National Laboratory, personal communication (1977).

35. J. Terrell, "Prompt Neutrons from Fission," Proc. of the IAEA Symposium on the Physics and Chemistry of Fission, Salzburg (1965), Vol. II, p.3.

36. R. Bois and J. Frehaut, "Evaluation Semi-Empirique de $\bar{\nu}_p$ pour la Fission Induite par Neutrons Rapides," Commissariat a l'Energie Atomique report CEA-R-4791 (1976).

37. J. Frehaut, G. Mosinski, R. Bois, and M. Soleilhac, "Mesure du Nombre Moyen $\bar{\nu}_p$ de Neutrons Prompts Emis Au Cours de la Fission Induite dans ^{240}Pu et ^{241}Pu par des Neutrons d'Energie Comprise Entre 1.5 et 15 MeV," Commissariat a l'Energie Atomique report CEA-R-4626 (1974).

38. D. DeVroey, A. T. G. Ferguson, and N. Stanfelt, "A Measurement of $\bar{\nu}$ for Neutron-Induced Fission of ^{240}Pu," J. Nucl. En. A/B20, 191 (1966).

39. F. Manero and V. A. Konshin, "Status of the Energy Dependent $\bar{\nu}$-Values for the Heavy Isotopes (Z > 90) from Thermal to 15 MeV and of $\bar{\nu}$-Values for Spontaneous Fission," At. En. Rev. 10, 637 (1972).

40. R. J. Howerton, "$\bar{\nu}$ Revisited," Nucl. Sci. Eng. 62, 438 (1977).

41. M. S. Krick and A. E. Evans, "Delayed-Neutron Yield vs. Energy Measurements," Trans. Am. Nucl. Soc. 13, 746 (1970).

Printed in the United States of America. Available from
National Technical Information Service
US Department of Commerce
5285 Port Royal Road
Springfield, VA 22161

Microfiche $3.00

001-025	4.00	126-150	7.25	251-275	10.75	376-400	13.00	501-525	15.25
026-050	4.50	151-175	8.00	276-300	11.00	401-425	13.25	526-550	15.50
051-075	5.25	176-200	9.00	301-325	11.75	426-450	14.00	551-575	16.25
076-100	6.00	201-225	9.25	326-350	12.00	451-475	14.50	576-600	16.50
101-125	6.50	226-250	9.50	351-375	12.50	476-500	15.00	601-up	

Note: Add $2.50 for each additional 100-page increment from 601 pages up.